Available online at www.eccomasproceedia.org
Eccomas Proceedia COMPDYN (2017) 297-314

ECCOMAS
Proceedia

COMPDYN 2017
6th ECCOMAS Thematic Conference on
Computational Methods in Structural Dynamics and Earthquake Engineering
M. Papadrakakis, M. Fragiadakis (eds.)
Rhodes Island, Greece, 15–17 June 2017

NUMERICAL STUDY OF THE BEARING CAPACITY AND MODES OF BUCKLING FAILURE OF A METAL SCAFFOLDING UNIT SUBJECTED TO VERTICAL COMPRESSION

George C. Manos[1] , V. Soulis[2], A. Nalmpantidou[3], V. Kourtides[4]

[1] Professor and ex-Director of the Lab. of Strength of Materials and Structures, Aristotle University
e-mail: gcmanos@civil.auth.gr

[2] Dr. Civil Engineer, Lab. of Strength of Materials and Structures, Aristotle University
e-mail: vassilios_soulis@yahoo.com

[3] Postgraduate student, Lab. of Strength of Materials and Structures, Aristotle University
e-mail: a.nalbantidou@gmx.de

[4] Dr. Civil Engineer, Research Ass., Lab. of Strength of Materials and Structures, Aristotle University

Keywords: Metal Scaffolding, Construction of Bridges, Failure Tests, Numerical Simulation

Abstract. *This paper presents results from an experimental and numerical investigation that was initiated from the failure of a complex scaffolding 3-D frame that was used at the construction site of a highway bridge overpass in Greece. This 3-D complex scaffolding frame was erected utilizing typical scaffolding units used by the construction industry in Greece made of steel tubular cross-sections. The tested scaffolding unit specimens were the same as the commercial units that were used in the failed 3-D scaffolding structure. A typical scaffolding unit consists of two towers 2.5 m high and 1.2 m wide, joined together by diagonal bracing. Two such prototype scaffolding units were tested by subjecting them to gradually increased compressive load up to failure. The tested specimens were were loaded vertically in compression. A special fixture was introduced at the top level so as to introduce a relatively flexible horizontal restraint to the tested scaffolding unit at this level and to ensure the vertical application of the load. Moreover, an effort was made to partly investigate the influence of the support conditions of the tested scaffolding units at the laboratory in order to examine the effect of such an influence on the response of the 3-D complex scaffolding structure in-situ. Finally, results from a non-linear inelastic numerical analysis, aimed to predict the behavior of the tested scaffolding units, are also presented. The obtained measured response is presented and discussed in terms of measured load-deformation response curves and observed modes of buckling failure. It can be seen from these results that realistic modes of failure were obtained by the adopted testing arrangement. Moreover, by comparing the obtained during testing bearing capacity and modes of failure with the corresponding results obtained from the non-linear inelastic numerical analysis reasonably good agreement could be reached. This supports the validity of the utilized numerical simulation.*

Peer-review under responsibility of the organizing committee of COMPDYN 2017.
doi: 10.7712/120117.5422.17894

1 INTRODUCTION

The majority of construction operations involve the use of scaffolding systems to support loads from activities that take place during construction (fresh concrete placement, workers, formwork, etc.). The construction phase of a project is commonly the period where structural failures due to scaffolding occur. The scaffolding must be able to withstand the superstructure and horizontal loads as well as the additional hydraulic pressure of fresh cement ([1], [2], [3]). It takes at least ten hours or more for the concrete to harden before it can carry its own weight. Before that, it relies on the scaffolding to hold it in place (figure 1a). From statistical data it can be concluded that a large part (50%) of human accidents in the construction industry are due to some type of scaffolding failure (figure 1b).

Figure 1a. Bridge overpass construction [4]

Figure 1b Penang second bridge collapse, in Malaysia, June 2013 [4]

Considerable attention is given in constructing in-situ the 3-D scaffolding support system by properly connecting the scaffolding units following a semi-empirical conservative scaffolding construction approach. This approach is usually conservative, especially when the supported parts are not extremely heavy and the scaffolding is founded on firm non-deformable soil. However, one cannot exclude uncertainties relevant to either the weight amplitude of the supported members or/and the scaffolding system boundary conditions.

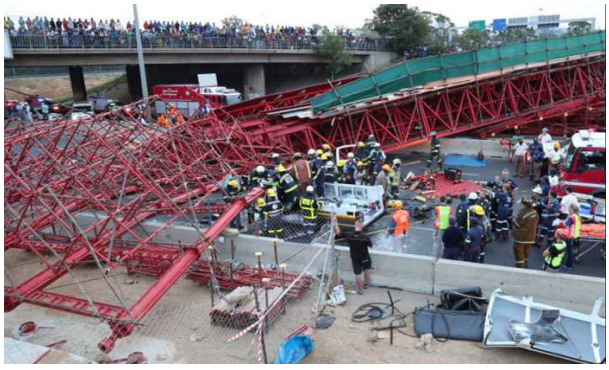

Figure 2. Scaffolding collapse on 14 October 2015 of Grayston bridge being constructed over the M1 in Sandton, South Africa [4].

Scaffolding failures [4] are usually due to overweight or support displacements when the supports of the scaffolding are founded on deformable media. In this case, unless stringent precautionary measures are taken, displacements of these scaffolding supports can influence significantly the transfer of loads and result in load transfer redistribution and overstressing of certain parts of the 3-D scaffolding structure. Such force redistribution and over-stressing can lead to large plastic deformations on various parts of the 3-D scaffolding structure and trigger partial or total collapse. Bridge collapses during construction, like the ones depicted in figures 1b, 2 and 3, demonstrates the importance of a conservative estimation of the load bearing ca-

pacity of scaffolding as well as of stringent supervision of the construction of such 3-D scaffolding structures, especially when is founded on deformable media.

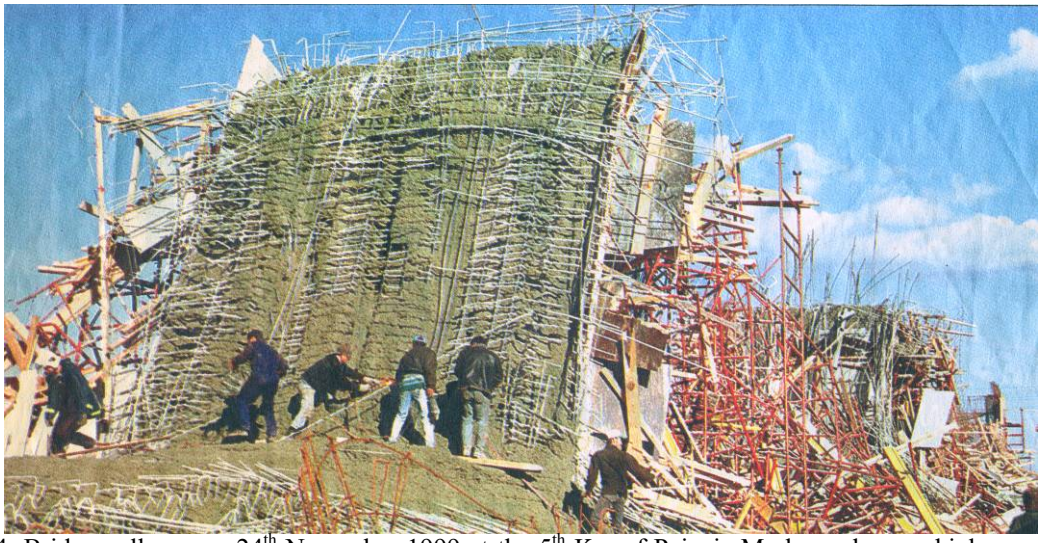

Figure 4. Bridge collapse on 24th November 1999 at the 5th Km of Paiania-Markopoulo new highway at Attiki Odos due to scaffolding failure

This paper's objective is to identify the load bearing capacity, and the modes of failure of a typical frame scaffolding used for construction practices in Greece. This is done through an experimental analysis, which took place in the Laboratory of Strength of Materials, in the Department of Civil Engineering, at Aristotle University of Thessaloniki. Moreover, a complementary numerical analysis was also carried out. A numerical investigation of a scaffolding structure was conducted by Peng et al. ([6], 1996) by examining through a computer simulation the behaviour of a three storey scaffolding representing actual construction practices. The numerical results show good agreement with the measurements of the behaviour obtained experimentally. The same authors ([7], 1996) simplify this numerical simulation in order to study the collapse of multi-bay scaffold systems; they present a simplified numerical treatment, and provide practical tools, such as guidelines and checklists, to ensure the safety of scaffold systems during construction. Weesner, and Jones ([8], 2001), studied experimentally and numerically the load bearing capacity of frame scaffolding. Four different types of frame scaffolding systems were tested experimentally, while commercially available software, capable of performing eigen-buckling and geometrically nonlinear analysis, was utilized to predict the ultimate load- carrying capacity of each scaffolding frame separately and compare the numerical predictions with the obtained measured values. In the present study, the behaviour of simple approximately 1000mm long tubular members, cut from typical scaffolding units, is first presented. The behaviour of these tubular members is studied numerically as well as by testing them when subjected to axial compression in the laboratory. Moreover, a 3-D scaffolding structure that is formed by two planar scaffolding tubular frames with all the connecting features is also examined when subjected to axial compression. This 3-D scaffolding structure is a typical scaffolding unit that formed the complex 3-D scaffolding structure that supported in-situ and failed during the construction of the bridge over-pass of figure 3. This typical scaffolding unit is tested under vertical compression in the laboratory up to failure. Next, its behaviour is also numerically simulated and compared to the measured response.

2 SIMPLE TUBULAR SECTIONS

Two tubular member specimens made of mild steel were tested. Initially they were of the same length, approximately 990mm. However, the first specimen was supported in such a way in the loading apparatus that its end supports should be considered as being fixed whereas the second specimen was provided in its end with two steel spherical supports. In this way its actual length was extended to be equal to 1080mm. The fixed tubular member cross-section had a mid-diameter equal to 45.5mm and a wall thickness equal to 2.5mm. The tubular member circular cross-section had a mid-diameter equal to 26mm and a wall thickness equal to 2.0mm. Figures 4a and 4b depict the fixed and pinned scaffolding tubular members when subjected to axial compression at the Laboratory of Strength of Materials and Structures of Aristotle University. The applied axial load together with the vertical displacement of the tubular member was monitored during testing

Figure 4a. Fixed scaffolding tubular member.

Figure 4b. Pinned scaffolding tubular member

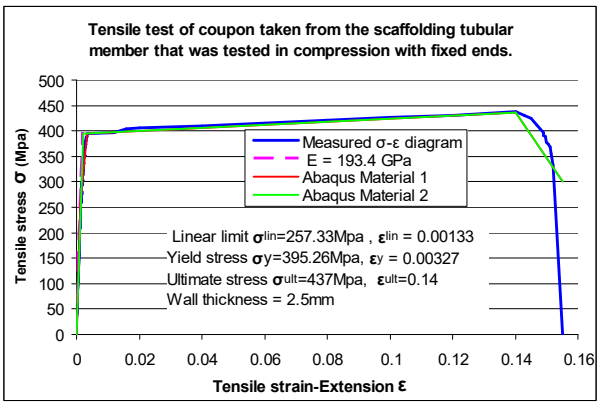

Figure 5a. Tensile coupon taken from fixed specimen.

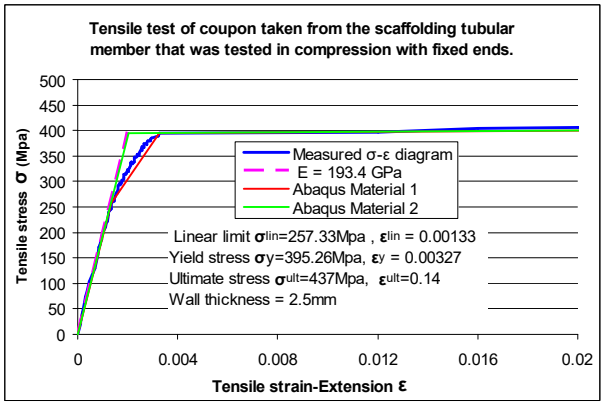

Figure 5b. Tensile coupon taken from fixed specimen.

The behaviour of these scaffolding tubular members under axial compression was also simulated numerically. This was done by a 3-D numerical simulation where all the geometrical features for these tubular members were exactly portrayed. At the same time the mechanical properties of the steel that these tubular members were made of was also exactly represented. Towards this end appropriate coupons for defining the material properties through an axial tensile test were taken from the same tubular members. The results of these

tensile tests, in terms of axial tensile stress-axial tensile strain diagram, together with the stress-strain values of particular significance (Linear limit, yield stress, ultimate stress) and the value of the Young's Modulus (E) are given in figures 5a, 5b and 6a, 6b for the fixed and pinned tubular member, respectively. These measured tensile steel properties were used in the numerical simulation through the ABAQUS software [11]. As can be seen in figures 5a and 6a the measured stress-strain diagram was approximated very closely by the stress-strain law that was used as input in this software. Figures 5b and 6b depict a comparison between the strain-stress law denoted as Material 1 and Material 2 that were used as input for the Abaqus software in simulating numerically the behaviour of the fixed and pinned scaffolding tubular members, respectively. As can be seen in these figures (5b and 6b) Material 1 follows more closely the measured stress-strain diagram than Material 2, which assigns a yield strain according to the measured yield stress and Young's Modulus.

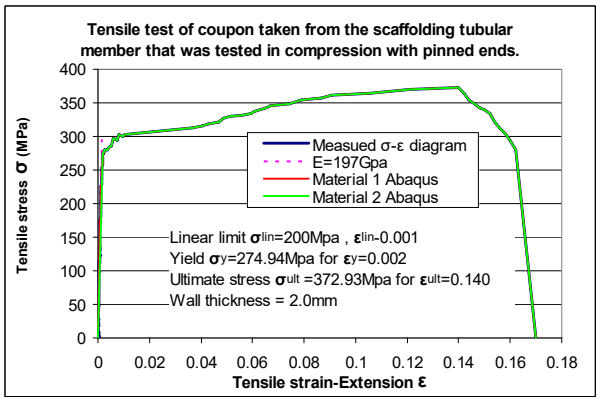

Figure 6a. Tensile coupon taken from pinned specimen.

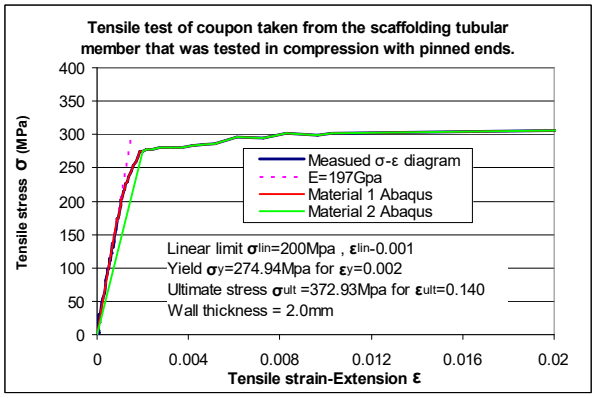

Figure 6b. Tensile coupon taken from pinned specimen.

Based on the above Material 1 and Material 2 stress (σ) strain (ε) diagrams that were derived from the corresponding measured tensile coupon behaviour taken from either the fixed or the pinned scaffolding tubular members the true stress (σ_t) against the true strain (ε_t) diagram were derived as they are utilized by the Abaqus software [11] (G.C. Manos et al. 2015, [13]). These Material 1 and Material 2 the true stress (σ_t) against the plastic strain (ε_p) diagrams are depicted in figures 7a and 7b for the scaffolding tubular fixed or pinned members, respectively. These diagrams were based on the definition of true stress (σ_t) and true strain (ε_t), which is given by the following relationships 1 to 3 (where the ε_y yield strain):

$$\sigma_t = \sigma (1 + \varepsilon) \qquad (1). \qquad \varepsilon_t = \ln (1 + \varepsilon) \qquad (2). \qquad \varepsilon_p = \varepsilon_t - \varepsilon_y \qquad (3).$$

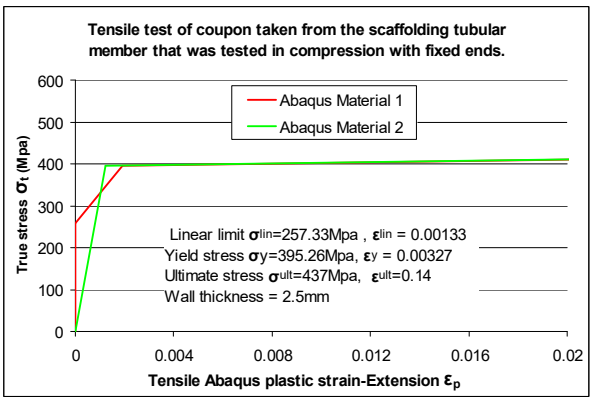

Figure 7a. True stress-strain diagram for fixed specimen.

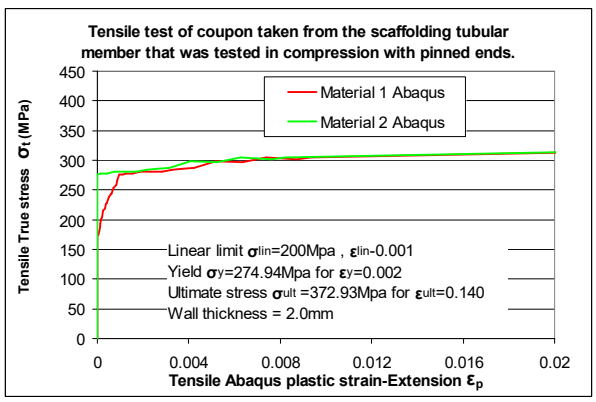

Figure 7b. True stress-strain diagram for pinned specimen.

Based on the above information that was used as input for the steel stress-strain properties that were utilized by the Abaqus software the numerical simulation of the scaffolding tubular members, either with fixed or with pinned ends, was carried out when they were subjected to vertical axial load.

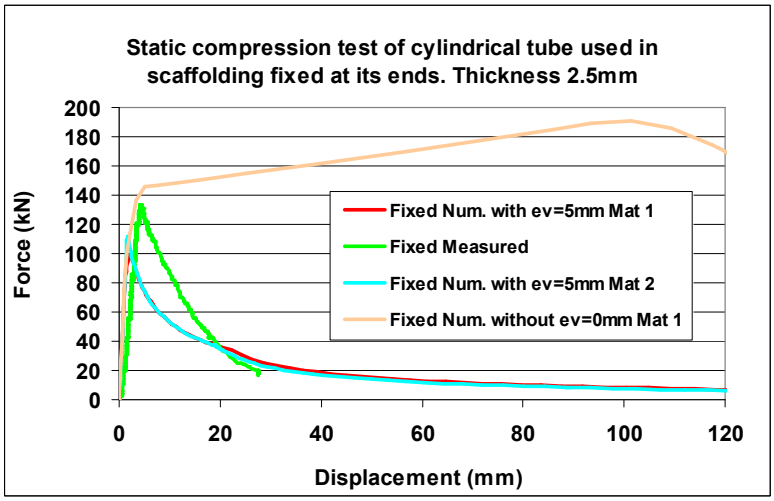

Figure 8a. Numerical and experimental behaviour of the fixed scaffolding tubular member under axial compression

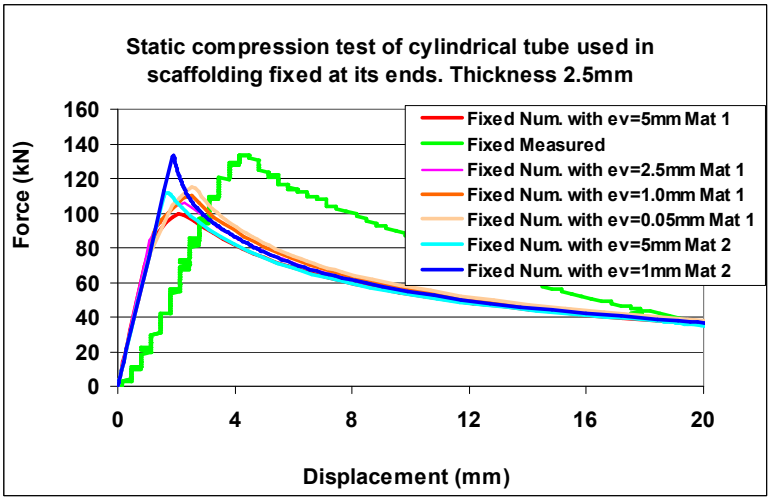

Figure 8b. Numerical and experimental behaviour of the fixed scaffolding tubular member under axial compression

The obtained numerical predictions of the behaviour of the tested scaffolding tubular members with fixed ends subjected to axial compression is depicted in figures 8a and 8b. Figure 8b is similar to figure 8a with a different scale for abscissas. The predicted load-displacement response, depicted in figure 8a, is obtained first when the axial load is applied centrally with zero eccentricity (e_v=0) and secondly when the value of this eccentricity is e_v =5.0mm; this is done employing either Material 1 or Material 2. These eccentricity values were determined following the relevant provisions of [5, 9, 10]. In the same plots the axial compression behaviour, measured during testing, is also plotted. In figure 8b, the sensitivity of the predicted response is studied by varying the employed eccentricity value. When Material 1 is employed this variation ranges from 5mm to 0.05mm whereas when Material 2 is employed this variation ranges from 5mm to 1mm. The measured and numerically predicted bearing capacity values are also listed in Table 1. As can be seen in figure 8a, the ideal zero eccentricity condition results in overestimating considerably the bearing capacity in axial compression of the

examined fixed tubular member by 43.3%. Moreover, the predicted limit behaviour in this case is the axi-symmetrical wrinkling and bulging of the thin wall near the two ends (see figure 10a). This is not in agreement with the observed bucking mode of failure (figure 10b). Moreover, as can be seen in figure 8b, the resulting bearing capacity is more sensitive to the value of the adopted eccentricity (e_v) for Material 2 than for Material 1. For Material 2 and for eccentricity e_v=1.0mm a very good agreement between the predicted and the measured axial load bearing capacity is obtained (see also table 1).

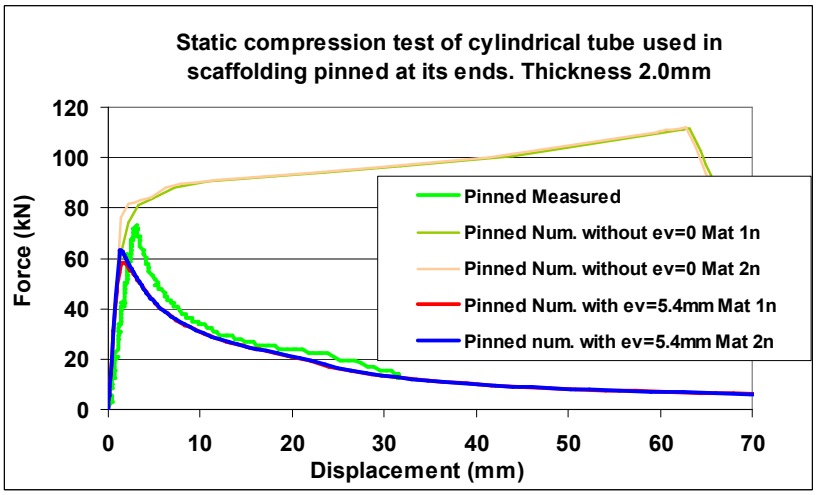

Figure 9a. Numerical and experimental behaviour of the pinned scaffolding tubular member under axial compression

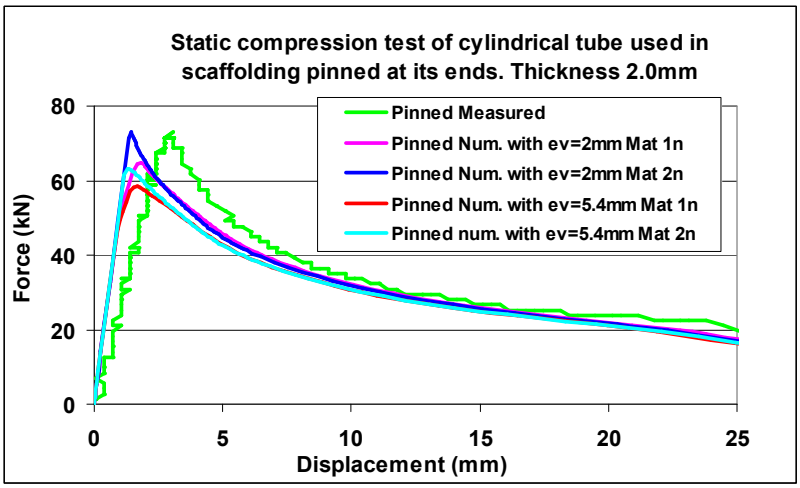

Figure 9b. Numerical and experimental behaviour of the pinned scaffolding tubular member under axial compression

The obtained numerical predictions of the behaviour of the tested scaffolding tubular members with pinned ends subjected to axial compression is depicted in figures 9a and 9b. Figure 9b is similar to figure 9a with a different scale for abscissas. In figure 9a The predicted load-displacement response, which is depicted in figure 9a, is obtained first when the axial load is applied centrally with zero eccentricity (e_v=0) and secondly when the value of this eccentricity is e_v=5.4mm. This is done employing either Material 1 or Material 2. These eccentricity values were determined following the relevant provisions of [5, 9, 10]. In the same plots the axial compression behaviour, measured during testing, is also plotted. In figure 9b, the sensitivity of the predicted response is studied again by varying the employed eccentricity value

(e_v). When either Material 1 or Material 2 is employed this variation ranges from e_v equal from 5.4mm to 2.0mm. The measured and numerically predicted bearing capacity values are also listed in Table 1. As can be seen in figure 9a, ideal conditions with zero eccentricity (e_v =0)condition result again in overestimating considerably the bearing capacity in axial compression of the examined fixed tubular member by 52.9%. Moreover, the predicted limit behaviour in this case is the axi-symmetrical wrinkling and bulging of the thin wall of the tubular member near the two ends (see figure 10a). This is not in agreement with the observed bucking mode of failure (figure 10c). In addition, as can be seen in figure 9b, the resulting bearing capacity is less sensitive to the value of the adopted eccentricity (e_v) for Material 1 than for Material 2. For Material 2 and for eccentricity e_v =2.0mm a very good agreement between the predicted and the measured axial load capacity is obtained (see also table 1).

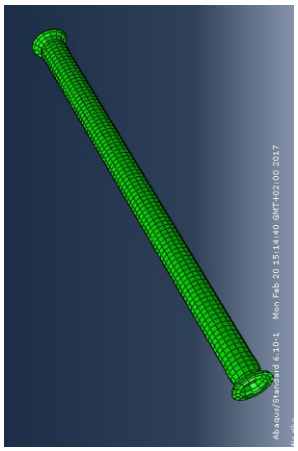

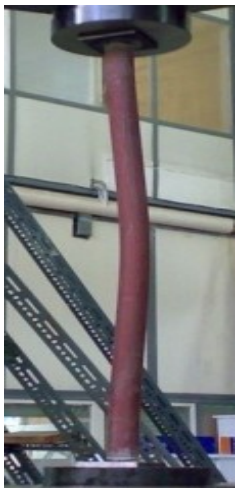

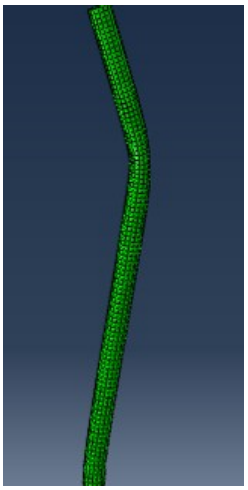

Figures 10a Zero eccentricity. 10b. Buckling of fixed end specimen 10c. Eccentricity e_v =5.0mm

Table 1. The measured and numerically predicted bearing capacity in axial compression of the tested scaffolding tubular members

Specimen	Numerical Prediction Bearing Capacity (KN) e_v =0	Numerical Prediction Bearing Capacity (KN) e_v >0	Measured Bearing Capacity (KN)
Fixed Ends	191.06 Mat 1 or Mat 2	99.43KN for e_v =4.95mm Mat 1 106.30KN for e_v =2.50mm Mat 1 109.96KN for e_v =1.00mm Mat 1 114.97KN for e_v =0.50mm Mat 1 133.62KN for e_v =1.00mm Mat 2 111.63KN for e_v =4.95mm Mat 2	133.29
Pinned Ends	111.55KN	58.45KN for e_v =5.40mm Mat 1 64.83KN for e_v =2.00mm Mat 1 63.25KN for e_v =5.40mm Mat 2 73.07KN for e_v =2.00mm Mat 2	72.95

For both the examined specimens (fixed or pinned) when the eccentricity values are based on the relevant provisions of [5], the numerically predicted bearing capacity is underestimated when compared with the measured bearing capacity (by 25.4% for the fixed end

specimen and by 21.3% for the pinned end specimen). At the same time, the predicted load-displacement response and mode of failure are in good agreement with the response of these specimens observed during testing. Moreover, adopting Material 2 (see figures 5a, 5b, 6a, 6b, 7a, 7b) instead of Material 2 yields better agreement between predicted and measured axial load bearing capacity. In addition, by adopting Material 2 the numerical simulation becomes more sensitive to the variation of the employed eccentricity value (e_v) than by adopting Material 1. Finally, based on the obtained numerical predictions it can be concluded that the studied numerical simulation procedure is a realistic approximation of the observed performance, in terms of load-displacement response and mode of failure of the tested scaffolding tubular members. The discrepancy observed between the predicted and observed bearing capacity values should be seen from the point of view that this underestimate is a reasonable additional safety feature.

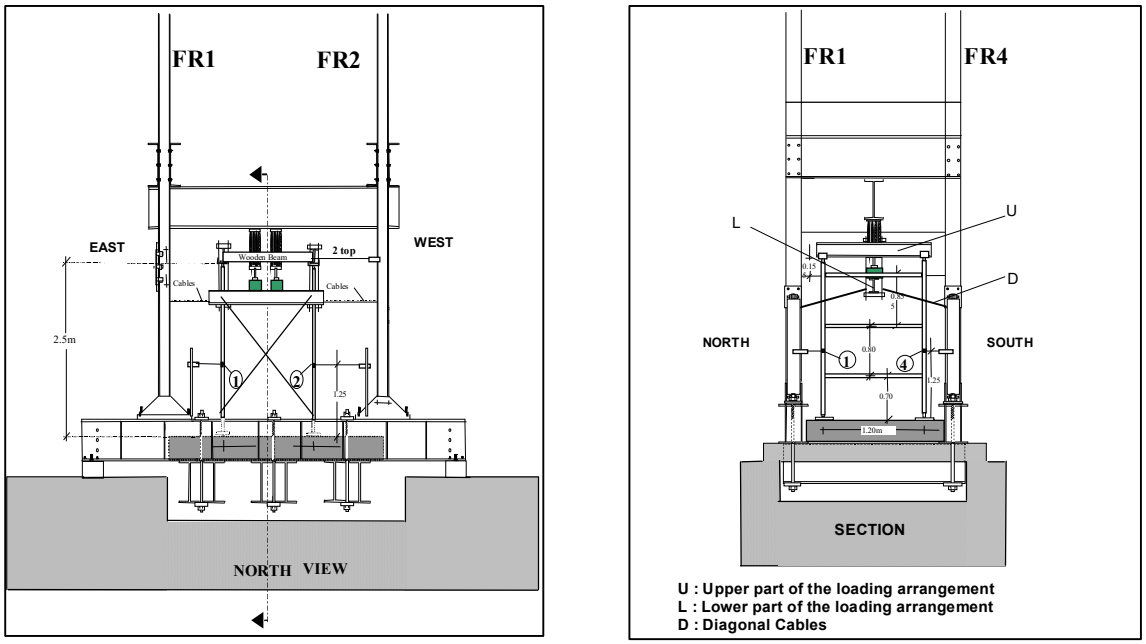

Figure 11. a) North view of experimental configuration. b) Section of experimental specimen

3 A 3-D SCAFFOLDING STRUCTURE UNIT – MEASURED PERFORMANCE

3.1 Description of the Used Loading Arrangement

The behaviour of a metal scaffolding, typical in Greek-practice, was examined under central vertical compression. The tested specimens were assembled by two towers 2.5m high and 1.2 m wide, joined together by x-bracing. The final specimen was 1500 mm long (Direction E-W), 1200 wide (Direction N-S) and 2500 mm high. The investigation was carried out at the Laboratory of Strength of Materials of Aristotle University of Thessaloniki (figures 11a and 11b). Two specimens of identical dimensions and manufacturing details were examined. The tested specimens were compressed centrally utilizing two vertical actuators of maximum capacity 196.2 KN each. These actuators were connected to a strong metal reaction frame. The supporting level of the scaffolding frame was located at the top of a strong RC reaction floor. At the top of the scaffolding frame, two 1.8m long top steel beams were spanning on top of each scaffolding tower (North-South direction) and formed the "upper part of the loading arrangement" (figure 11b). These beams were loaded symmetrically at mid-span, in such a way as to transfer the vertical load equally to the four legs of the scaffolding frame. This was achieved

by loading, through the two hydraulic actuators, a cross steel beam spanning between the top steel beams at mid-span (figures 11a and 11b). These top steel beams were also connected with two strong wooden planks spanning in the East-West direction, so as to form a relatively flexible upper horizontal support level. However, in order to prohibit excessive horizontal movements at the horizontal plane of applying the vertical loads, the cross steel beam was tied at its two ends by two diagonal cables. These cables were pre-stressed by a certain small force level after the whole loading arrangement has been checked for its symmetry and its plumberness prior to applying the load. This cross steel beam thus, was forming the "lower part of the loading arrangement" (figure11b). The actuators directly in contact with this cross beam exerted the compressive force to the scaffolding. This "lower part of the loading arrangement" was supported by two vertical hangers on the "upper part of the loading arrangement". The vertical hangers were assembled by a group of four vertical steel rods, and metal plates, that transferred the loads in a simply-supported way.

The overall specimen's behaviour, regarding its stability, was monitored by recording the load of each of the two actuators, and therefore the total load applied on the specimen, as well as the horizontal displacements of each of the four legs of the specimen. The horizontal displacements, were recorded at mid-height of the scaffolding's legs (1250mm from the base), as well as at the "upper part of the loading arrangement" for the 2nd specimen. (2600mm from the base), (see figures 12a, 12b, 13a, 13b).

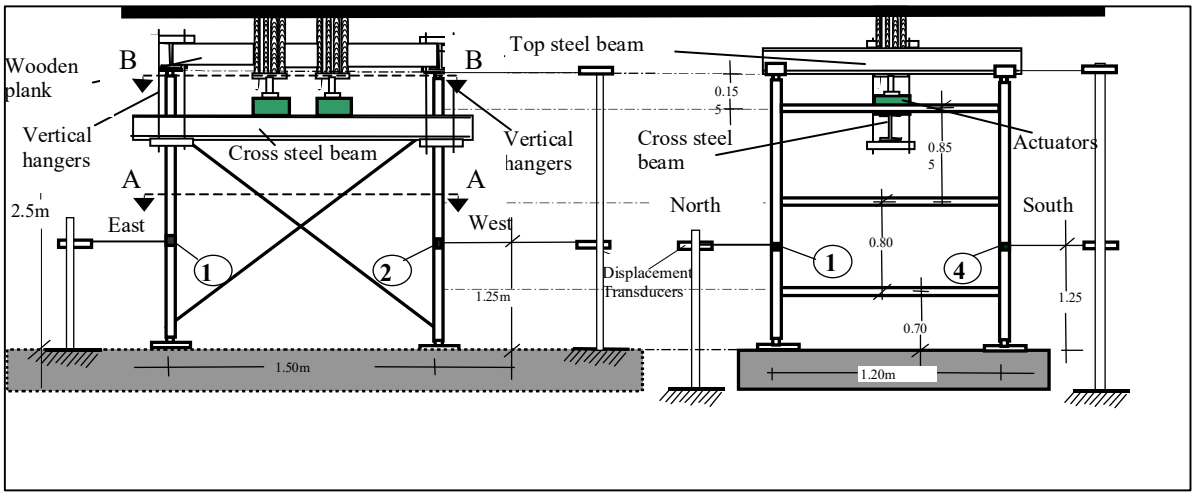

Figure 12. Loading arrangement for the scaffolding under central compression.

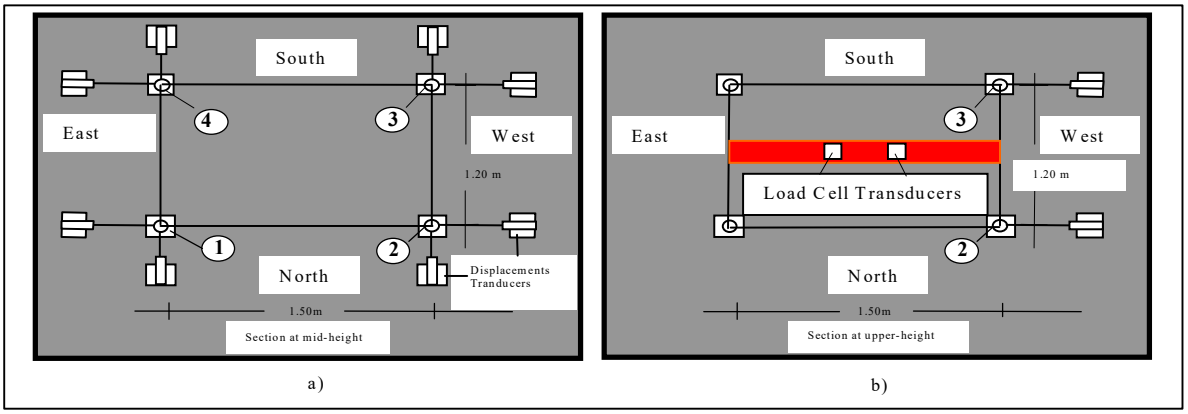

Figure 13. a) Plan of transducers position in scaffolds mid-height A-A. b) Plan of transducers position in scaffolds top level B-B.

3.2 Description of the Experimental Sequence and Observed Behaviour

During the experimental sequence a vertical compressive load was applied to the system, as described, at constant rate (figure 14). Successful tests were considered when the two actuators remained vertical through out the duration of the experiment. The load and the displacements were recorded by a multi-channel data acquisition system. The pre-buckling and post-buckling behaviour of the 3–D scaffolding unit, was recorded during four different tests. The first specimen was tested during Tests 1, 2, 3. For all these tests the scaffolding screw jack bases were in direct contact with the concrete slab. The second specimen was tested in the fourth test. In this case the scaffolding screw jack bases were resting on wooden planks that were placed on top of the concrete slab. The summary test results are depicted in figure 15. The performed tests are described in some detail in the following text.

Figure 14. 3-D Scaffolding unit at the loading frame

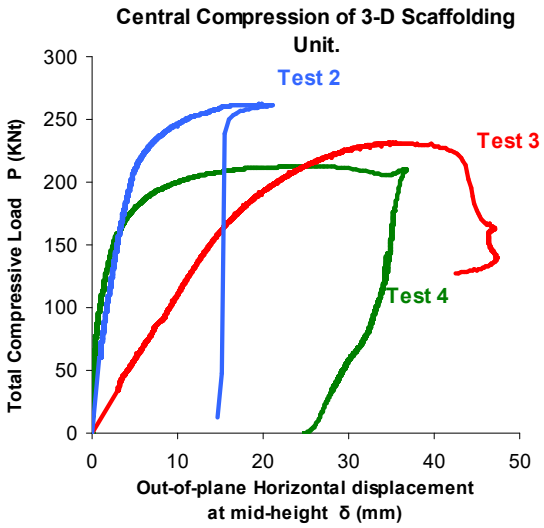

Figure 15. Test results from Central Compression

Test No1: This test was a preliminary elastic test where the maximum recorded total load was equal to 150 KN. This test represents a reference initial elastic test.

Test No2: This was a buckling test, whereby the loading was stopped almost as soon as the buckling of specimen was initiated. During this test, the maximum load that was recorded was equal to 255.06 KN. The horizontal displacement at mid height of the scaffolding legs exhibited a large increase at this stage. In order to plot the results in a summary form the total vertical load was obtained by the sum of the load applied by each actuator. In any case, the two actuators applied almost identical forces to the specimen. Moreover, an average value was obtained from the recorded horizontal displacement at mid- height (figure 15). This value was found by averaging all four recorded horizontal displacements at mid height in the East –West direction. This direction was chosen because the development of the buckling mode was most pronounced in this direction. The halting of load increase at this stage, was immediately followed by the removal of all compression from the specimen. The measured behaviour is depicted by the curve test 2 in figure 15. The horizontal displacements were more pronounced for legs 1 and 2 than for legs 3 and 4 (see figure 16a).

Test No3: The third test was a repeat buckling test again of specimen 1, which developed permanent deformations during test 2. Two additional instruments were placed at the upper part of the loading arrangement to monitor the East-West horizontal displacements at this level (figure 13b). During this test, this specimen developed large permanent plastic deforma-

tions that in the form of the predominant bucking mode (figure 16b). The maximum load this time was somewhat lower (215.82KN) than the one recorded during Test 2. The described before buckling mode (East to West) became more pronounced. The same vertical legs 1 and 2, which developed plastic deformations before, developed further permanent out-of plane deformations. Permanent deformations were also observed at the attachments between the top steel beams and the wooden planks. The cross bracings at the North and South elevations did not develop any visible sign of distress. Permanent deformations also developed at the scaffolding screw jack bases, which were in direct contact with the reinforced concrete strong floor slab.

Test No4: In this test, the behaviour of the second specimen was examined. During this test the load was applied continuously even beyond the stage where the maximum buckling load developed. Again the dominance of the East to West buckling mode was clearly observed. The maximum load, reached this time was approximately 215.82KN. This specimen developed large plastic deformations that led this specimen to form its bucking mode. The observed behaviour for specimen 2 during test 4 was very similar to the one observed during test 3 for the previous specimen 1. This time the screw jack bases did not developed any distress. Instead, the wooden inserts that were placed between these bases and the concrete slab exhibited, during to their flexibility, large permanent deformations. Despite the large horizontal permanent displacement of the vertical legs (mainly for legs 1 and 2) the cross bracings (North and South elevations) did not develop any visible sign of distress. Typical buckling mode shapes of tested specimens 1 and 2 can be seen in figures 16a and 16b.

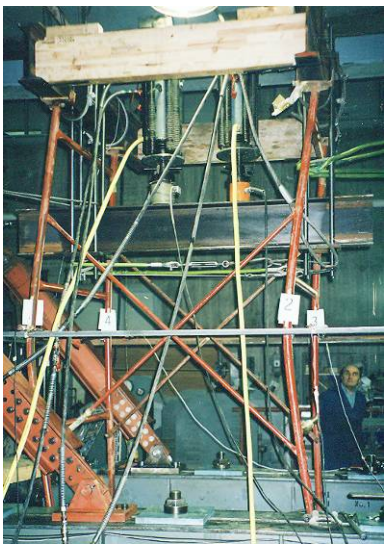

Figure 16a. Buckling shape of 1st specimen

Figure 16b. Buckling shape of 2nd specimen

4 A 3-D SCAFFOLDING STRUCTURE UNIT – NUMERICAL SIMULATION

A three-dimensional F.E numerical simulation of the scaffolding 3-D unit, the members of the loading arrangement, and the restraining system was formed aiming to predict the behaviour of the tested scaffolding unit. Two kinds of analysis were conducted to predict the bearing capacity of the scaffolding; that is first an eigen-buckling analysis and secondly a geometrically non-linear, material linear analysis [12]. In the case of the geometrically non -linear, material linear analysis, a small vertical eccentricity from the initially perfectly plumb position was introduced to the model in the East-West direction to establish the ultimate bearing capacity. The solution method utilized in performing the geometrically non-linear analysis was

the total Lagrangian method. Three dimensional thin beam elements were utilized to model the scaffolding 3-D unit. In addition, three-dimensional thick beam elements were used to model the cross bracing members and the diagonal cables in order to introduce special end releases at their edges. Thick beams were also used to model the upper & lower parts of the loading arrangement together with the vertical hangers. The numerical model was simply supported at the bottom parts of its four legs. The diagonal cables and braces were also assumed to be pin- connected at both ends. A preliminary sensitivity analysis took place to verify the influence of certain parameters of the support conditions and of the lower and upper part of the loading arrangement. This preliminary analysis demonstrated that the numerical simulation at the connections between the top steel beams, the top wooden planks, the hangers, and the lower cross beam at the described in section 3.1 loading arrangement had an influence on the numerically predicted bearing capacity. The following five distinct cases for the numerical simulation of these connections is presented and discussed below (see also figure 17).

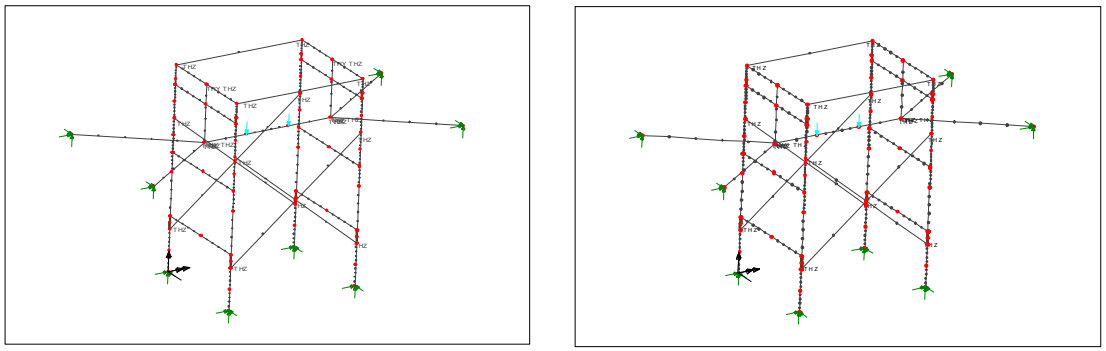

a) b)

Figure 17. a) Case 1 modeling b) Case 3 modeling

Case 1: In this case the vertical hangers are assumed to be fixed at the upper part of the loading arrangement and pinned at the lower part of loading arrangement. The top wooden planks are assumed to be rigidly connected to the upper part of the loading arrangement at their ends. The predicted behaviour is depicted by curve Case 1 in figure 18.

Case 2: This is identical to case 1 but in this case the vertical hangers are assumed to be pinned at both their ends at the upper and lower part of the loading arrangement. The Case 2 curve describes the overall vertical-load-horizontal displacement response.

Case 3: This is identical to case1 but both the top wooden planks are assumed to be pinned connected to the upper part of loading arrangement. The predicted behaviour is depicted by curve Case 3 in figure 18.

Case 4: This case is identical to case1 but the vertical hangers are assumed to be pinned at both their ends at the upper and lower part of the loading arrangement. The top wooden planks are assumed to be pinned connected to the upper part of loading arrangement. The predicted behaviour is depicted by curve Case 4 in figure 18.

Case 5: This is an additional analysis with the numerical model having the same simulation of the loading arrangement as Case 3. This time, however, the stiffness values of the various members found at the end of the eigen-value buckling solution of Case 3 were adopted here through a restart option of the used software. The objective here was to simulate the sequence

of testing between Test 2 and Test 3, as described in section 3.2, whereby the load was removed at the end of Test 2 when buckling was initiated and re-applied to the deformed structure at the beginning of Test 3. The predicted behaviour is shown in figure 18 (curve Case 5).

The obtained numerical predictions of the "Total Axial Vertical Load" versus the "Average out-of-plane Horizontal Displacement" numerically simulated response of the various examined connections are depicted in figure 18. As it becomes obvious from figure 17, the obtained axial load predicted capacity of the scaffolding 3-D unit is significantly influenced by the way the various connections were numerically simulated. This numerical investigation indicates that these connections of the scaffolding units in order to form the total 3-D scaffolding assembly will also bear a significant influence on the capacity of the whole structure.

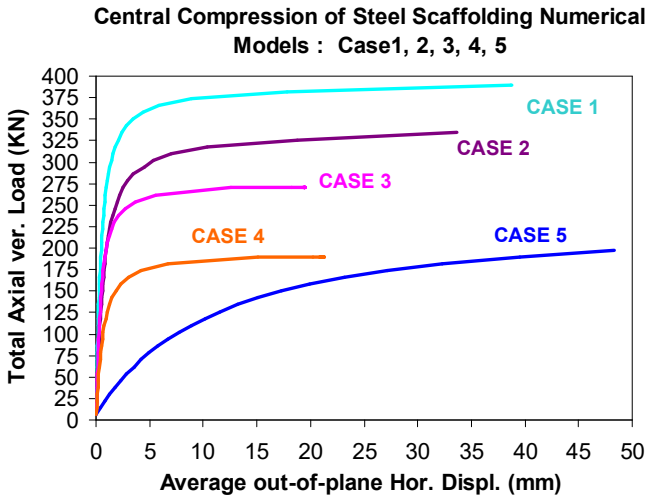

Figure 18. Test results from Central Compression

Table 2

Experimental bearing capacity and modes of failure

Test Number	Experimental results: Max Total Load (KN)	Mode of Buckling Failure
Test1	150.00	Elastic Behaviour
Test2	261.70	Predominant West-East
Test3	231.50	Predominant West-East
Test4	212.20	Predominant East-West

Table 3

Numerical bearing capacity and modes of Failure

Model	Eigen-Buckling Analysis: Total Load (KN)	Geometric Nonlinear analysis: Max Total Load (KN)	Average Horizontal Displacements and Rotations at start of Buckling: Start of Buckling	Top Height (mm)	Mid Height (mm)	Θz Rotations at Top-height	Mode of Buckling Failure
Case1	389.98	390.00	387.50	20.20	64.27	-0.1	East-West
Case2	335.64	336.60	329.84	22.89	59.30	-0.085	East-West
Case3	248.61	271.17	271.14	-1.69	18.22	-0.89	East-West
Case4	179.90	189.66	189.65	-1.15	20.22	-1.315	East-West
Case5		218.116	212.63	-24.62	97.375	-7.543	East-West

In tables 2 and 3, the maximum compressive load values are listed, either as applied during the experimental sequence or as obtained from numerical investigation. The buckling load levels, as obtained from the eigen-buckling analysis, are also listed. The primary mode of failure as observed in each case is also noted.

4.1 Comparison of Observed and Numerically Predicted Behaviour

In what follows the numerically predicted behaviour, which was obtained as described before, is compared with the observed behaviour. This comparison is three-fold. First, the measured bearing capacity under compression of the tested 3-D scaffolding unit is compared with the numerically predicted bearing capacity. This is done by comparing the relevant values listed in Tables 2 and 3. Secondly, this comparison effort is supplemented by comparing the numerically obtained "Total Axial Vertical Load" versus "Average out-of-plane Horizontal Displacement" response with the corresponding measured response. This is done in figure 19. Finally, this comparison is finalized by comparing the observed and the predicted buckling failure modes. This is done in tables 2 and 3 as well as by comparing the numerically predicted deformation patterns for maximum vertical load in figures 20a and 20b with the observed buckling shapes of the tested 3-D scaffolding units shown in figures 16a and 16b.

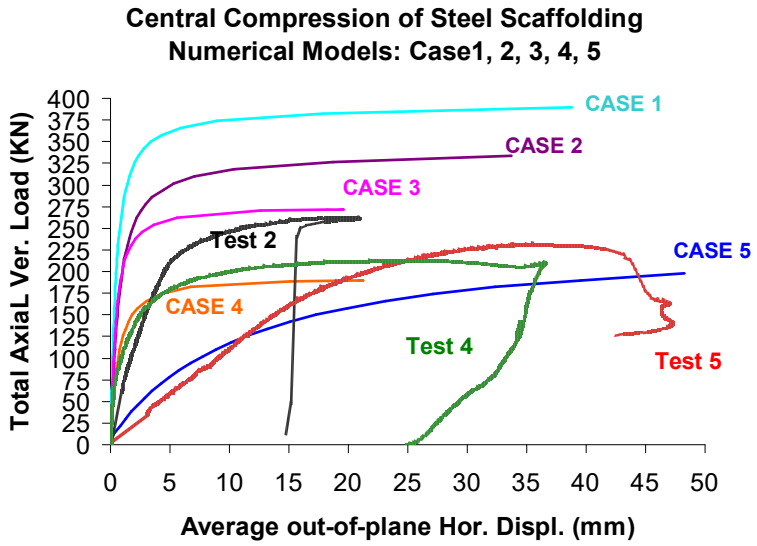

Figure 19. Measured and numerically predicted "Axial Load versus Horizontal out-of-plane displacement" response.

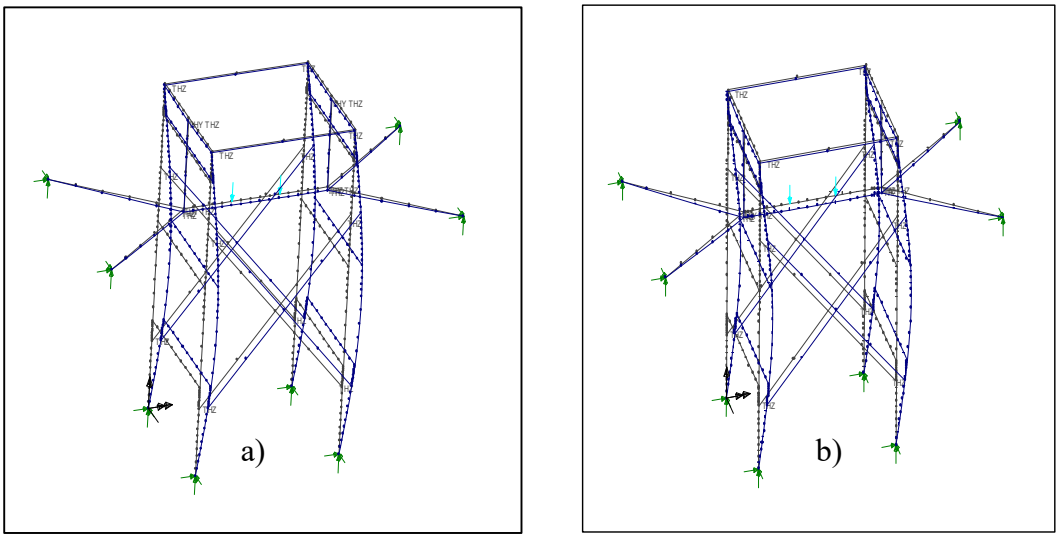

Figure 20 a) Primary buckling mode for Case 1. b) Primary buckling mode for Case 3

As can be seen from this comparison Case 1 is a rather stiffer simulation than either the observed behaviour or the response obtained from the rest of the numerical simulations (Cases 2, 3, 4 and 5). When buckling is initiated, the values of the top and mid-height average displacements of Case 1 model are lower than the ones obtained for Case 2 model (22.89 mm and 59.30mm for Case 1 as compared to 20.20mm and 64.27mm for Case 2). At the same time, the obtained for Case 1 bearing capacity value is the highest of all the numerical predictions (387.50KN). As listed in table 3, Case 2 model is also stiffer that the ones corresponding to Case 3, 4 or 5 models. Thus, it was demonstrated that the top wooden planks, when they are rigidly connected with the rest of the steel scaffolding frame, provide enough rotational restrain to result in a significant increase of the total bearing capacity. On the other hand, Case 3 and Case 4 numerical simulations allow wooden planks to rotate free about their z-axis at their ends. Both these cases, experience smaller top and mid-height horizontal displacements, but higher rotations at the top of scaffolding's leg as shown in table 3. They result in relatively lower values for the numerically predicted bearing capacity than the corresponding values predicted Case 1 and Case 2. Cases 1, 2, 3 and 4 numerical simulations exhibit the same buckling mode that has the form of large out-of-plane horizontal displacements from East to West leading to buckling instability and failure. However, Cases 1 and 3, whereby the hangers are modeled as rigidly connected members with the upper loading arrangement show higher stiffness than Cases 2 and 4. The Case 5 numerical simulation develops larger values for the out-of-plane horizontal displacements response, both at mid-height and at the top, than the corresponding values for Case 1 to 4 numerical models. Despite these large out-of-plane horizontal displacements Case 5 numerical model predicts larger value for the bearing capacity than Case 4 numerical model (218.116KN compared to 189.66KN, see table 3). The response, which was predicted for Case 5 numerical simulation, is also more flexible than the corresponding response predicted by numerical simulations Case 3 and 4.

The measured response during Test 2, which achieved the largest bearing capacity value (261.70KN), agrees quite well with the corresponding numerical predictions of Case 3 (248.61KN from the eigen-buckling analysis and 271.17KN form the geometrical non-linear analysis).

Comparing Test 2 with Test 4 it can be seen that a 20% higher buckling load was achieved during Test 2 than Test 4. These two tests were performed with identical specimens differing only at the type of support they utilized at their screw jack bases supporting the four legs of the 3-D scaffolding unit. For Test 4 the supports of the four legs of the scaffolding unit were resting on wooden planks thus representing more flexible supports than the corresponding support conditions that materialize for Tests 1, 2 and 3. This can be further verified by the fact that the steel screw jack bases during Test 4 were not permanently deformed whereas during Test 2, where the screw jack bases were in direct contact with the concrete slab, permanent deformation occurred at these steel bases. This fact indicates that a high degree of restrain was present during Tests 2 and 3 rather than in Test 4. Therefore a departure from the pinned end condition should be assumed for Tests 2 and 3 whereas for Test 4 the pinned end support conditions can be accepted as a realistic assumption.

The behaviour obtained by the rest of the examined numerical models also demonstrate the effect of the restrains either at the top of the 3-D scaffolding unit exercised by the wooden planks or from the support of the four legs at the base. The less flexible the support conditions at the base of the 3-D scaffolding unit or/and the stiffer the restrain exercised by the wooden planks at the top of the 3-D scaffolding unit result in higher bearing capacity values for the 3-D scaffolding unit when subjected to compressive loads.

From this discussion it can be concluded that such an extensive parametric numerical investigation complemented by the corresponding testing sequence can unfold the sensitivity of the

bearing capacity of the examined 3-D scaffolding unit to the restrain conditions either at the top or at the bottom leg supports. It can also be concluded that when these top-restrain or bottom support flexibility conditions can be realistically modeled then the resulting numerical predictions, in terms of bearing capacity values, load-displacement response and failure modes, are well in agreement with the observed behaviour. In this way, such investigation can be seen as a process in validating numerical tools so that these tools can be subsequently utilized with confidence for the design of scaffolding structures.

5 CONCLUSIONS

1. Simple or complex scaffolding units were studied first by subjecting them to axial compression and then by non-linear numerical simulations utilizing commercial software.
2. It was demonstrated both from the extensive parametric numerical investigation complemented by the corresponding testing sequence that the bearing capacity of the examined 3-D scaffolding unit was influenced significantly by the restrain conditions either at the top or/and at the bottom leg supports.
3. Therefore, it can be concluded that when these top-restrain or bottom support flexibility conditions can be realistically modeled then the resulting numerical predictions, in terms of bearing capacity values, load-displacement response and failure modes, are well in agreement with the observed behaviour.
4. In this way, such investigation can be seen as a process in validating numerical tools so that these tools can be subsequently utilized with confidence for the design of scaffolding structures.

ACKNOWLEDGEMENTS

The authors would like to thank George Penelis, Professor Emeritus of Aristotle University for the opportunity to participate in this investigation.

- To the memory of Ray W. Clough, Professor Emeritus of the University of California, at Berkeley, U.S.A.

REFERENCES

[1] EN 12811-1, (2003): Temporary works equipment, Part 1: Scaffolds!–Performance requirements and general design.

[2] EN 12812 (2004): False work, Performance requirements and general design.

[3] EN 12813 (2004): Temporary works equipment, Load bearing towers of prefabricated components, Particular methods of structural design.

[4] https://www.google.gr/Scaffolding and construction failures

[5] EN 1993-1-1 (2005): Eurocode 3: Design of steel structures - Part 1-1: General rules and rules for buildings. Abs 532(3).

[6] Peng JL, Pan AD, Rosowsky DV, Chen WF, Yen T, Chan SL. High clearance scaffold systems during construction – I. Structural Modeling and modes of failure. Eng Struct, 1996;18(3): 247-57.

[7] Peng JL, Pan AD, Rosowsky DV, Chen WF, Yen T, Chan SL. High clearance scaffold systems during construction – II. Structural analysis and development of design guidelines. Eng Struct, 1996; 18(3): 258-67.

[8] Weesner LB, Jones HL. Experimental and analytical capacity of frame scaffolding. Eng Struct, 2001; 23(3): 592-99.

[9] Nethercot DA. Limit states design of structural steelwork. Chapman & Hall, (1991). UK.

[10] Owens GW, Knowles PR. Steel designers' Manual. The steel construction institute. (eds. Blackwell Science), UK. (1992).

[11] Hibbitt, Karlsson, Sorensen. Inc. ABAQUS user's manual volumes I–V and ABAQUS CAE manual. Version 6.10.1. Pawtucket, USA; 2010.

[12] LUSAS Release 13.2-3. Lusas Modeller Reference Manual. UK: FEA Ltd, 2000.

[13] G.C. Manos, A. Nalmpantidou, V. Kourtides, A. Anastasiadis "Cyclic Response of a Steel Beam-to-Column Connections – An Experimental and Numerical Study", COMPDYN 2015, Greece, 25–27 May 2015.